Effect of Cesium Substitution on the Superconducting Properties of Bi-2212 samples prepared via solid state reaction and laser floating zone technique

I.Ergin[1], B. Özçelik[1*], M. A. Madre[2], A. Sotelo[2]

[1]Department of Physics, Faculty of Sciences and Letters, Cukurova University. 01330 Adana, Turkey

[2]ICMA (CSIC-Universidad de Zaragoza). María de Luna, 3. 50018 Zaragoza, Spain

Abstract

In this work, the effect of cesium substitution on the structural and superconducting properties of $Bi_2Sr_2Ca_{1-x}Cs_xCu_2O_y$ (where x = 0.0, 0.025, 0.050, 0.075, 0.10, 0.125, and 0.15) samples prepared by the solid-state reaction route and by directional growth using the laser floating zone (LFZ) technique has been studied. X-ray diffraction has shown that both kinds of samples present the 2212 phase as the major one, with pseudo tetragonal structure, accompanied by minor amounts of $(Sr,Ca)CuO_2$ and $Bi_2(Sr,Ca)_4O_{6+\delta}$ secondary phases. SEM-EDX results indicate that Bi-2212 phase is the major one, with small amounts of secondary phases. Cs substitution diminishes the size and content of secondary phases. Magnetization measurements reflect different behavior for sintered and LFZ grown samples. Although the diamagnetic transition is very wide for the former samples, it is very sharp for the last ones. The critical onset temperatures, T_C, are around 80 and 90 K, for sintered and LFZ grown samples, respectively. Moreover, M–H measurements indicate that LFZ grown samples exhibit larger areas than the sintered ones. The intragranular critical current, J_C, calculated from the M–H loops and Bean's formula, is maximum for x = 0.025Cs sintered and x = 0.05Cs LFZ grown samples. The maximum pinning forces, F_{Pmax}, determined in these samples are higher than those obtained in undoped ones, reaching 9×10^7 Oe*A/cm^2 and 10×10^8 Oe*A/cm^2, at 10 K, for sintered and LFZ grown samples, respectively.

Keywords: Bi-2212; Cesium substitution; Magnetic properties; Laser floating zone technique

1 Introduction

HT_c superconductor materials consist of different families, and among them, the Bi-Sr-Ca-Cu-O (BSCCO) is one of the most studied. This family can be described by the $Bi_2Sr_2Ca_{n-1}Cu_nO_{2n+4+y}$ general formula, where n = 1, 2, and 3, being n the number of CuO_2 layers in the crystal structure, producing the Bi-2201, Bi-2212, and Bi-2223 phases. These phases arecharacterized by different critical temperatures (T_C) about 20, 85, and 110 K, respectively, where these phases undergo from the normal to the superconducting state [1,2]. As it is well known, the Bi-2212 phase is known as the most stable high-T_c one, in a wide range of compositions and processing temperatures. On the other hand, the critical temperature of Bi-2212 phase is significantly influenced by the chemical doping or elementary substitutions. When Bi and Ca contents are reduced, provided that the oxygen content is constant, T_c values are remarkably increased [3]. Since their discovery, researchers have performed many experimental efforts in order to better understand the relationship between their microstructure and physical properties, trying to improve their T_c and critical current density, J_C (maximum current transported by the material without passing to the normal state), for technological applications [4–14].

Besides, BSCCO family has excellent advantages like high critical magnetic field (H_c), high critical temperature, and high critical current density. On the other hand, it has also some drawbacks, like weak links, high anisotropy, and small coherence length. Therefore, these disadvantages limit their technological applications. Generally, very small misorientation of grains in this system causes a drastic drop of J_C values. In order to overcome those disadvantages, different strategies have been tested to exploit their high anisotropy by aligning their grains along the conducting planes, decreasing the effect of anisotropy and weak links [15–17].

The laser floating zone (LFZ) technique is very effective to obtain a good grain orientation in Bi-2212 superconductors [4–6,15–17]. In this technique, extremely high thermal gradients are produced in the solidification front, leading to a preferential alignment of grains with their c-axis perpendicular to the growth direction [18], maximizing the transport properties along the growth axis.

In addition, alkaline metal substitution in this BSCCO system has pointed out that the disorder produced by their incorporation in the crystal structure

influences the critical temperature, since their ionic radii (73–181 pm) are similar to those of Bi, Sr, Ca, and Cu. Moreover, alkaline metals have +1 valence state; hence, the alkaline earth substitution leads to a modification of the charge carrier concentration. The substitution of alkaline metals for Bi, Sr, and Cu in BSCCO superconductor was performed by several authors [19–21], showing that while T_C was increased by Li and Na substitution, it was decreased by K and Rb. Furthermore, it has also been determined that alkaline metals drastically decrease the formation temperature of the Bi-2212 phase. In addition, in the best of our knowledge, no studies about the Cs substitution effect on the Bi-2212 properties have been studied. As a consequence, the purposes of the present work are:

1. Introducing optimum amounts of Cs into the $Bi_2Sr_2Ca_{1-x}Cs_xCu_2O_{8+y}$ system by replacing Ca due to their similar ionic radii but different oxidation states. As it is known, Ca has an oxidation state +2 while Cs is +1. As a result, modifications can be produced in the crystal structure, together with changes in carrier concentration due to variations in oxygen content.
2. Exploring the structural, electrical, and magnetic behavior of these modified systems, compared with the undoped one.
3. Evaluating the results as a function of Cs concentration, as all these mentioned effects should lead to modifications of the superconducting and magnetic properties of the system.

For this purpose, different substitutions have been performed in the $Bi_2Sr_2Ca_{1-x}Cs_xCu_2O_{8+y}$ (where x = 0.0, 0.025, 0.050, 0.075, 0.10, 0.125, and 0.15). Moreover, the effect of grain alignment has been also studied by comparing sintered (pellet) samples prepared by the classical solid-state reaction and textured fibers produced through the LFZ technique.

2 Experimental Details

$Bi_2Sr_2Ca_{1-x}Cs_xCu_2O_{8+y}$ samples, with x = 0.0, 0.025, 0.05, 0.075, 0.1, 0.125, and 0.15, have been prepared by using the well-known ceramic route. Appropriate amounts of commercial fine powders Bi_2O_3 (Sigma-Aldrich, 99.9%), $SrCO_3$ (Sigma-Aldrich, + 98%), $CaCO_3$ (Sigma-Aldrich, + 99%), Cs2O (Sigma-Aldrich, + 98%), and CuO (Sigma-Aldrich, 99%) were milled in an agate mortar and calcined twice at 750 and 800 °C for 12 h in order to decompose the

carbonates. It is necessary to emphasize here that the two-step calcination process is very important for materials which are processed using the LFZ technique. If carbonates are present in the mixture, they decompose inside the molten zone, creating some bubbles and destabilizing the crystallization front [22], leading to grain misorientations and parasitic grain growth. In addition, some amount of the free CO_2 can be trapped inside the material, increasing porosity and/or decreasing the grain connectivity. The calcined powders were then pressed into 10-mm-diameter pellets at 4–6 tons, and sintered in a tubular furnace under air by two steps: 60 h at 860 °C, followed by 12 h at 800 °C, and, then, quenched in air to room temperature.

For the LFZ process, calcined powders were isostatically pressed in form of cylinders of 2–3 mm diameter under 200 MPa. The green ceramics obtained were used as feed in the LFZ installation [23], using a continuous power Nd:YAG laser (λ = 1064 nm), under air, at a growth rate of 30 mm/h, producing very homogeneous dimensionally cylindrical bars (~ 2 mm diameter and 120 mm length). On the other hand, Bi-2212 ceramic presents incongruent melting, producing different secondary phases as Bi-2201, $CaCuO_2$, or $(Sr,Ca)CuO_2$ [24] after solidification. As a consequence, after the directional solidification process, it is necessary to perform a thermal treatment to form the Bi-2212 phase from the secondary ones [25]. The annealed process was applied under air and consisted in two steps: 60 h at 860 °C, followed by 12 h at 800 °C, and, finally, quenched in air to room temperature.

In order to identify the phases, powder X-ray diffraction patterns of the materials were recorded at room temperature using a Rigaku Miniflex diffractometer system, working with CuKα radiation and a constant scan rate between 2θ = 3°–70°. SEM micrographs were taken using a LEO Evo-40 VPX scanning electron microscope (SEM) fitted with an energy dispersive spectrometry (EDS) analysis system. Magnetic measurements were carried out in a 7304 model Vibrating Sample Magnetometer of Lake Shore. The $Bi_2Sr_2Ca_{1-x}Cs_xCu_2O_{8+y}$ samples (x = 0.0, 0.025, 0.050, 0.075, 0.10, 0.125, and 0.15) prepared by solid-state route and LFZ technique will be hereafter named as bulk (pellet) and fiber, respectively.

3 Results and Discussion

Powder X-ray diffraction was performed on all samples in order to determine the variations of structure and crystal parameters arising from Cs substitution. The XRD patterns for bulk and fiber samples with different Cs substitutions are shown in Fig. 1 a and b, respectively. As it can be easily seen in these graphs, major peaks are associated with the superconducting Bi-2212 phase, with pseudo tetragonal crystal symmetry. Calculated lattice parameters by using the least square method are tabulated in Tables 1 and 2. The uncertainty of the crystal lattice parameter calculation remained in the ± 0.001 range. As it can be easily observed in the tables, the processing technique has negligible influence on these parameters. On the other hand, when comparing both types of samples, Bi-2201 and $SrCuO_2$ secondary phases are identified in bulk samples, while only $CaCuO_2$ secondary phase is found in fibers.

In order to obtain more information about the crystal sizes in the samples, the Debye-Scherrer formula [26] has been used:

$$L_{hkl} = 0.9\lambda/\beta cos\theta \quad (1)$$

where λ is wavelength, β is the full width at half maximum, and θ is the angle of the peak. The obtained results are presented in Tables 1 and 2, for the bulk and fiber samples, respectively. From these data, it is clear that the processing technique has a significant influence on the crystal size, being about two times larger for samples prepared through the LFZ technique. The largest crystallite sizes were found as 289 Å for bulk 0.075Cs substituted sample and 548 Å for 0.05Cs fiber one.

In Fig. 2 a–c and d–f, the surface morphologies of bulk and fiber samples, respectively, are presented. In these micrographs, it can be seen that both bulk and fiber samples present different contrasts related, through EDS, to different phases. Major contrast in all samples (indicated by #1) is the gray one, corresponding to the superconducting Bi-2212 phase. White (#2) and dark gray (#3) ones are the $Bi_2(Sr,Ca)_4O_{6+\delta}$ and $(Sr,Ca)CuO_2$ secondary phases, respectively. Moreover, Cs addition clearly increases porosity in bulk samples, while no evident modification is produced in fiber ones. In addition, it can be clearly observed that Cs substitution increases the secondary phase sizes in bulk samples, while the opposite effect is produced in fibers. Another difference

between bulk and fiber samples is the random orientation of grains in the former ones, while long and well-oriented grains are produced in the fibers.

In Fig. 3 a and b, the magnetization, M, versus temperature, T, for bulk and fiber samples obtained under 50 Oe applied magnetic field are presented, respectively. All magnetization data were recorded by cooling the sample in zero field down to 10 K, then applying 50 Oe magnetic field, and collecting data on warming up to 100 K. As it can be seen in the graphs, the general behavior of magnetization related to bulk and fiber samples are completely different. Very wide diamagnetic transition is obtained in bulk samples, while it is very sharp for the fiber ones. The critical onset temperatures, T_C, corresponding to the diamagnetic transition, and determined from these data are presented in Tables 1 and 2, for the bulk and fiber samples, which are around 80 and 90 K, respectively. In addition, the onset temperature of bulk samples monotonically increases with Cs substitution, while it increases up to x = 0.05Cs and then gradually decreases in the fiber ones. These effects are due to the granular nature of samples; thus, as a result, the grain boundaries show strong connectivity and, therefore, the magnetic field does not easily penetrate into the sample.

The M–H loops measured at 10 K and between ± 1 T applied external fields, under ZFC mode, are presented in Fig. 4 a and b. The results demonstrate that fiber samples exhibit larger areas when compared to the bulk ones. The loop areas increase up to x = 0.025Cs and x = 0.05Cs for the bulk and fiber samples, respectively. From these M–H data, the intragranular J_C values of bulk and fiber samples have been calculated using the critical Bean model [27]:

for bulk $J_c = 20\left(\frac{\Delta M}{\alpha\left(1-\frac{\alpha}{3b}\right)}\right)$ (2)

for fibers $J_c = 30\frac{\Delta M}{d}$ (3)

respectively where J_C is known as the critical current density in amperes per square centimeter of a sample. $\Delta M = M+ - M-$ is measured in electromagnetic units per cubic centimeter, a and b are the length of the sample plane perpendicular to the applied magnetic field, and d is the sample thickness. Figure 5a and b show the calculated critical current density values at 10 K, up to 1 T, for bulk and fiber samples. In the figures, it can be observed that the

intragranular critical current calculations yield that the x = 0.025Cs bulk and x = 0.05Cs fiber samples present the largest J_C values, 23 × 10^3 A/cm^2 and 25 × 10^4 A/cm^2, at zero magnetic field, respectively. These results indicate that J_C values of fiber samples are 10 times higher than those of bulk ones, due to the better grain alignment obtained in the former ones. On the other hand, critical current density values decrease when the magnetic field and the amount of Cs are increased. It can be argued that the secondary phases in the matrix may cause such a kind of behavior. In the granular high-T_c superconducting material, the non-superconducting phases situated in the main matrix may behave as very effective flux-pinning centers. Depending on the sizes of those impurities, the applied fields start to penetrate into the sample and reduce the critical current values. The maximum J_C values obtained in textured samples are about two times higher than the reported in LFZ grown Na-doped materials (1.33 × 10^5 A/cm^2) [16]. This fact can be due to the different sizes of both cations (1.67 and 1.02 nm for Cs^+ and Na^+, respectively), which can affect the oxygen content and the charge carrier mobility. Moreover, the lower effective attraction of the external electrons in the Cs^+ cations can be responsible of a possible slight charge carrier concentration enhancement.

It is known that the intrinsic properties of pinning centers like size, capability, stability, and density directly affect the flux pinning force, F_P. Therefore, in order to deeply analyze the nature of vortex pinning mechanism in the bulk and fiber samples, it is necessary to calculate the pinning forces by using $F_P = J_c \times \mu_0 H$ equation [28]. The results are exhibited in Fig. 6 a and b, for bulk and fiber samples, at 10 K, respectively. As it can be seen in the figures, the pinning force, F_P, values regularly increase for low applied magnetic fields, and then start sharply to decrease above 8000 Oe, for all samples. The F_{Pmax} values of x = 0.025Cs in bulk (9 × 10^7 Oe*A/cm^2) and x = 0.05Cs in fibers (10 × 10^8 Oe*A/cm^2) are higher than the values determined in undoped ones (≈ 7.5 × 10^7 Oe*A/cm^2). All the results are tabulated in Tables 1 and 2 for the bulk and fiber samples. It is necessary to emphasize here that the pinning force of fiber samples is about 10 times larger than in bulk ones, indicating that the LFZ technique improves the superconducting properties compared to the solid-state reaction.

In order to better understand the nature of pinning mechanism of x = 0.025Cs bulk and x = 0.050Cs fiber samples, the experimentally obtained data have been analyzed by using the Dew-Hughes model [28] in which the reduced pinning force F_P/F_{Pmax} with respect to reduced field $b = H/H_{max}$ is drawn as shown in Fig. 7 a and b, together with their fitting with equation f_P (F_P/F_{Pmax}) = $b^p(1-b)^q$. For high-T_C bulk superconductors, three theoretical models [29] are used to identify the pinning mechanism introduced below as:

$f_P(b) = 25-16b^{-1/2}\ (1-b/5)^2$; normal surface pinning (2)

$f_P(b) = 9/4b(1-b/3)^2$; normal point pinning (3)

$f_P(b) = 3b^2(1-2b/3)$; Δk pinning (4)

It can be observed that the experimental findings for x = 0.025Cs bulk and x = 0.050Cs fiber samples are well-matched with the normal point pinning in the limited scale.

4 Conclusions

In summary, a comparative study of structural, physical, and magnetic properties of cesium-substituted Bi-2212 phase synthesized by conventional solid-state and laser floating zone (LFZ) technique has been done. X-ray diffraction patterns showed that both bulk and fiber samples contain Bi-2212 phase as the major one. SEM micrographs and EDX results have proven that Bi-2212 was the major phase, accompanied by minor amounts of $(Sr,Ca)CuO_2$ and $Bi_2(Sr,Ca)_4O_{6+\delta}$ secondary phases. Bulk and fiber samples behave differently with respect to the magnetization versus temperature characterization. The diamagnetic transition was very wide for bulk samples, while it was very sharp for the fiber ones. The critical onset temperatures, T_C, for the bulk and fiber samples are around 80 and 90 K, respectively. M–H measurements showed that the fiber samples exhibit larger loop areas than the bulk ones. J_C is maximum for the x = 0.025Cs bulk and x = 0.05Cs samples, 23 × 10^3 A/cm^2 and 25 × 10^4 A/cm^2, respectively. These results indicate that J_C values of fiber samples are 10 times higher than those of bulk samples. The highest pinning forces have been determined in x = 0.025Cs bulk and x = 0.050Cs fiber samples, 9 × 10^7 Oe*A/cm^2 and 10 × 10^8 Oe*A/cm^2, at 10 K, respectively. The pinning force of fiber samples is about 10 times larger than

the bulk ones. This situation may be accepted as an indication of the enhancement of the energy barriers arising from the increment of Cs content, resulting an increasing of the pinning centers. These pinning centers behave as effective pinning centers; therefore, the penetration of the applied magnetic field is not allowed into the sample. In addition, the increment of the critical current, J_c, values are obtained to point out the indication of the strong pinning mechanism originated from Cs substitution. In this case, an increment of the intergranular coupling and a decrease of the number of weak links are revealed. Moreover, in both cases, pinning centers show a normal point pinning nature. All these results clearly point out that the LFZ technique drastically improves the superconducting properties when compared with the measured in sintered samples prepared through the classical solid-state reaction.

Acknowledgments

The authors wish to acknowledge the use of Servicio General de Apoyo a la Investigación-SAI, Universidad de Zaragoza.

Funding Information

This work is supported by Research Fund of Çukurova University, Adana, Turkey, under grant contract no. FYL-2018-9926. M. A. Madre and A. Sotelo recognize the MINECO-FEDER (MAT2017-82183-C3-1-R) and Gobierno de Aragon-FEDER (Research Group T 54-17 R) for funding.

References

1. Michel, C., Herviev, M., Borel, M.M., Grandin, A., Deslands, F., Provost, J., Raveav, B.: Z. Phys. B. 86, 421 (1987)

2. Maeda, H., Tanaka, Y., Fukutumi, M., Asano, T.: Jpn. J. Appl. Phys. 27, 209 (1988)

3. Majewski, P., Su, H.L., Quilitz, M.: J. Mater. Sci. 32, 5137 (1997)

4. Özçelik, B., Kaya, C., Gündoğmuş, H., Sotelo, A.,Madre,M.A.: J. Low Temp. Phys. 174, 136 (2014)

5. Özaslan, A., Özçelik, B., Özkurt, B., Sotelo, A., Madre, M.A.: J. Supercond. Nov. Magn. 27, 53 (2014)

6. Gündoğmuş, H., Özçelik, B., Sotelo, A., Madre, M.A.: J. Mater. Sci. Mater. Electron. 24, 2568 (2013)

7. Lennikov, V., Özkurt, B., Angurel, L.A., Sotelo, A., Özçelik, B., de la Fuente, G.F.: J Supercond.Nov. Magn. 26, 947 (2013)

8. Sotelo, A.,Mora, M., Madre,M.A., Diez, J.C., Angurel, L.A., de la Fuente, G.F.: J. Eur. Ceram. Soc. 25, 2947 (2005)

9. Mora, M., Sotelo, A., Amaveda, H., Madre, M.A., Diez, J.C., Angurel, L.A., de la Fuente, G.F.: Bol. Soc. Esp. Ceram. V. 44, 199 (2005)

10. Nane, O., Özçelik, B., Sotelo, A., Madre, M.A.: J. Eur. Ceram. Soc. 37, 1007–1012 (2017)

11. Özçelik, B., Nane, O., Sotelo, A., Amaveda, H., Madre, M.A.: J. Mater. Sci. Mater. Electron. 28, 6278–6283 (2017)

12. Laliena, C., Amaveda, H., Özçelik, B., Martínez, E., de la Fuente, G.F., Angurel, L.A.: Ceram. Int. 44, 14865–14872 (2018)

13. Özçelik, B., Gürsul, M., Nane, F.K., Madre, M.A., Sotelo, A.: J. Mater. Sci. Mater. Electron. 29, 19147–19154 (2018)

14. Bal, S., Dogruer, M., Yıldırım, G., Varilci, A., Terzioglu, C., Zalaoglu, Y.: J. Supercond. Nov. Magn. 25, 847 (2012)

15. Costa, F.M., Ferreira, N.M., Rasekh, S., Fernandes, A.J.S., Torres, M.A., Madre, M.A., Diez, J.C., Sotelo, A.: Cryst. Growth Des. 15, 2094 (2015)

16. Nane, O., Özçelik, B., Amaveda, H., Sotelo, A., Madre, M.A.: Ceram. Int. 42, 8473 (2016)

17. Sotelo, A., Ozcelik, B., Amaveda, H., Bruned, A., Madre, M.A.: Ceram. Int. 41, 14276 (2015)

18. de la Fuente, G.F., Ruiz, M.T., Sotelo, A., Larrea, A., Navarro, R.: Mater. Sci. Eng. A. 173, 201 (1993)
19. Sykorova, L.D., Smrckova, O., Jakes, V.: Phys. Status Solidi C. 1(7), 1952 (2004)
20. Kawai, T., Horiuchi, T., Mitsui, K., Ogura, K., Takagi, S., Kawai, S.: Physica C. 161, 561 (1989)
21. Bilgili, O., Selamet, Y., Kocabas, K.: J. Supercond. Nov.Magn. 21, 439 (2008)
22. Sotelo, A., Rasekh, S., Madre,M.A., Diez, J.C.: J. Supercond. Nov. Magn. 24, 19 (2011)
23. Carrasco, M.F., Costa, F.M., Silva, R.F., Gimeno, F., Sotelo, A., Mora, M., Diez, J.C., Angurel, L.A.: Physica C. 415, 163 (2004)
24. Mora, M., Sotelo, A., Amaveda, H., Madre, M.A., Diez, J.C., Capel, F., Lopez-Cepero, J.M.: J. Eur. Ceram. Soc. 27, 3959 (2007)
25. Costa, F.M., Silva, R.F., Vieira, J.M.: Physica C. 323, 23 (1999)
26. Cullity, B.D.: Element of X-ray diffraction. Addison-Wesley Publishing Company Inc., Boston (1956)
27. Bean, C.P.: Phys. Rev. Lett. 8, 250 (1962)
28. Dew-Hughes, D.: Philos. Mag. 30, 293 (1974)
29. Sharma, D., Kumar, R., Awana, V.P.S.: Ceram. Int. 39, 1143 (2013)

Table 1 T_C values deduced from the dc M–T measurement data, unit cell parameters, crystal size, maximum pinning force, and critical current density of bulk samples

Concent. x	*Tc (K)*	*Unit-cell parameter a=b (Å)*	*Unit-cell parameter c (Å)*	*Cyrstal size L_{hkl} (Å)*	*F_{pmax} at 10 K($x10^7$ Oe*A/cm^2)*	*Jc ($x10^3$ A/cm^2)*
x=0	80	5.41	30.67	279	7.26	22.07
x=0.025	80.1	5.41	30.70	277	8.99	23.02
x=0.05	80.3	5.41	30.74	272	5.75	16.77
x=0.075	80.5	5.40	30.70	289	2.51	10.01
x=0.1	81	5.41	30.70	247	3.15	8.47
x=0.125	82	5.41	30.70	224	1.64	7.34
x=0.15	84	5.41	30.69	269	0.85	6.2

Table 2 T_C values deduced from the dc M–T measurement data, unit cell parameters, crystal size, maximum pinning force, and critical current density of fiber samples

Concent. x	*Tc (K)*	*Unit-cell parameter a=b (Å)*	*Unit-cell parameter c (Å)*	*Cyrstal size L_{hkl} (Å)*	*F_{pmax} at 10 K ($x10^7$ Oe*A/cm^2)*	*Jc ($x10^4$ A/cm^2)*
x=0	91	5.41	30.70	521	7.93	19.13
x=0.025	91.5	5.41	30.70	529	9.33	23.27
x=0.05	92	5.42	30.71	548	10.08	25.62
x=0.075	91	5.41	30.73	433	7.87	19.32
x=0.1	90	5.41	30.73	481	5.41	13.87
x=0.125	89	5.41	30.71	417	3.14	9.14
x=0.15	85	5.41	30.70	505	2.02	5.82

Figure captions

Figure 1. XRD patterns of (***a***) bulk; and (***b***) fiber samples. Peaks corresponding to the Bi-2212, Bi-2201, and $SrCuO_2$ phases are indicated by 2, *, and **o** respectively.

Figure 2. SEM micrographs of the $Bi_2Sr_2Ca_{1-x}Cs_xCu_2O_y$ samples with x = ***a)*** 0.00 bulk; ***b)*** 0.075 bulk; ***c)*** 0.15 bulk; ***d)*** 0.00 fiber; ***e)*** 0.075 fiber; and ***f)*** 0.15 fiber.

Figure 3. Magnetization against temperature ***a)*** bulk; and ***b)*** fiber samples, for the different Cs-content

Figure 4. *M-H* loops for ***a)*** bulk; and ***b)*** fiber samples measured at 10 K.

Figure 5. Calculated critical current densities, J_c, of the ***a)*** bulk and ***b)*** fiber samples, as a function of the applied magnetic field, at 10K.

Figure 6. Pinning Force versus applied field for ***(a)*** bulk; and ***(b)*** fiber samples, at 10K.

Figure 7. Reduced Pinning Force versus reduced applied field, for ***a)*** x=0.025Cs bulk; and ***b)*** x=0.05Cs fiber samples, at 10 K.

Figure 1

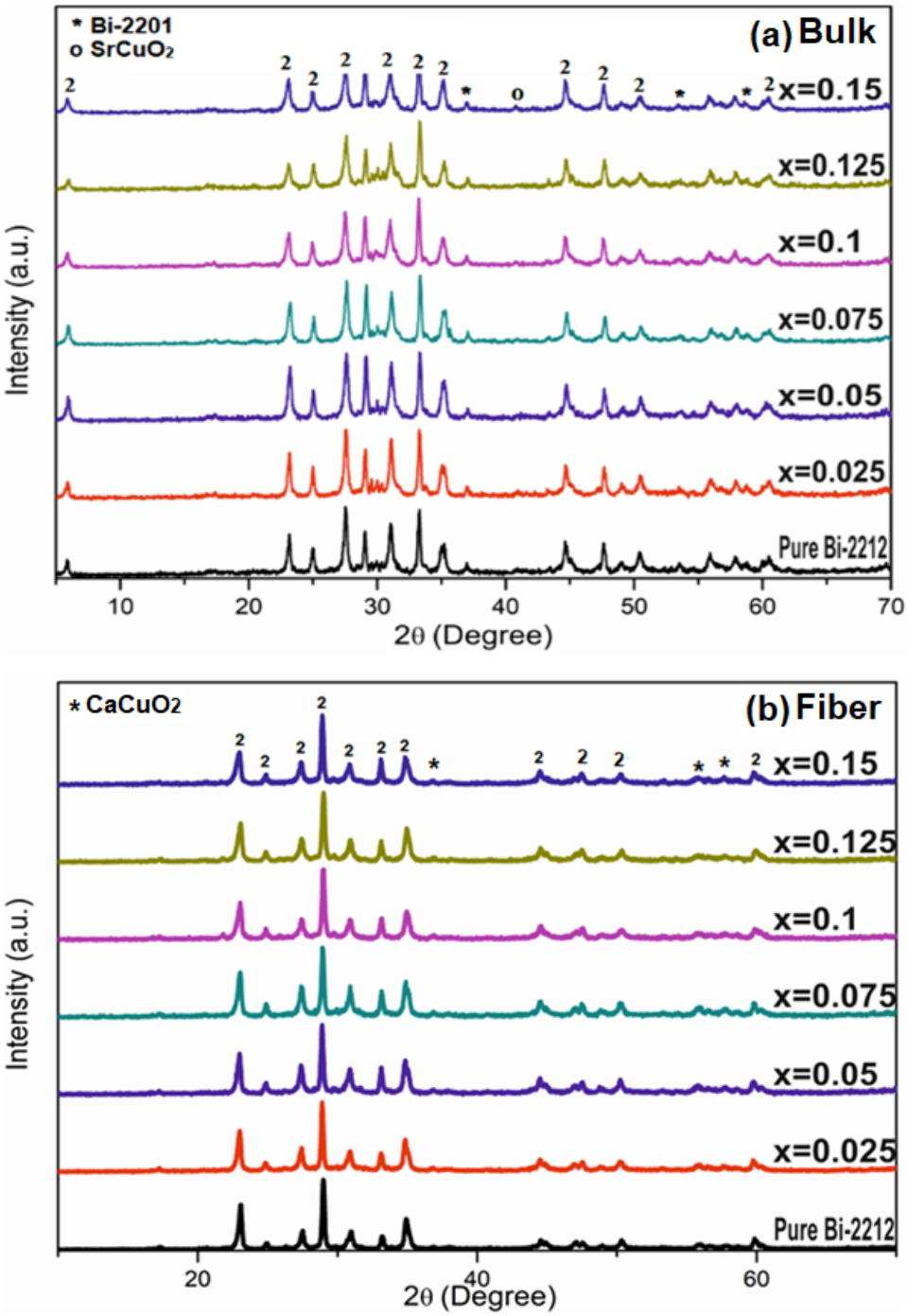
* Bi-2201
o SrCuO2
(a) Bulk
x=0.15
x=0.125
x=0.1
x=0.075
x=0.05
x=0.025
Pure Bi-2212
Intensity (a.u.)
10
20
30
40
50
60
70
2θ (Degree)
* CaCuO2
(b) Fiber
x=0.15
x=0.125
x=0.1
x=0.075
x=0.05
x=0.025
Pure Bi-2212
Intensity (a.u.)
20
40
60
2θ (Degree)

Figure 2

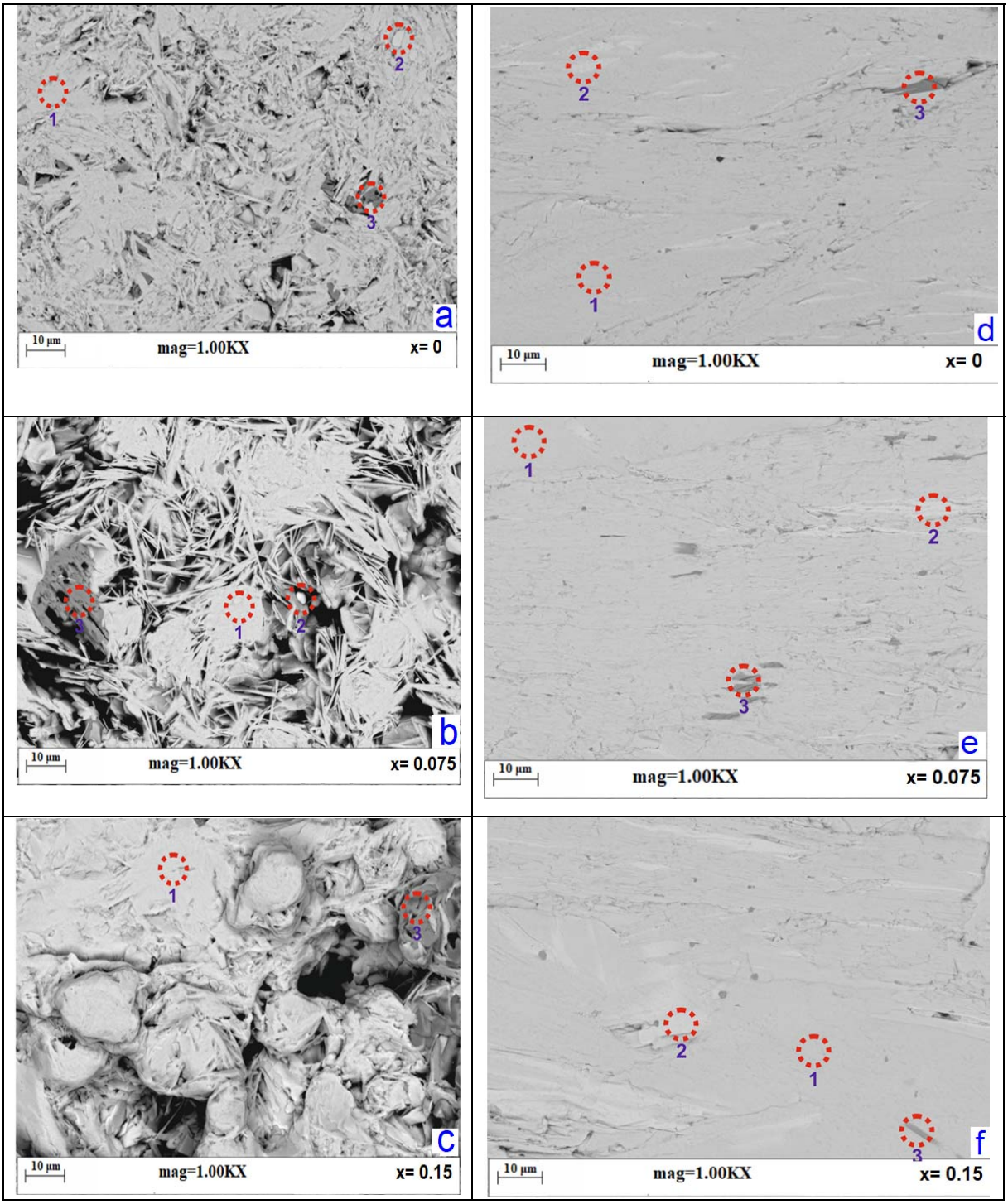
1
2
3
a
10 µm
mag=1.00KX
x= 0
2
3
1
d
10 µm
mag=1.00KX
x= 0
3
1
2
b
10 µm
mag=1.00KX
x= 0.075
1
2
3
e
10 µm
mag=1.00KX
x= 0.075
1
3
c
10 µm
mag=1.00KX
x= 0.15
2
1
3
f
10 µm
mag=1.00KX
x= 0.15

Figure 3

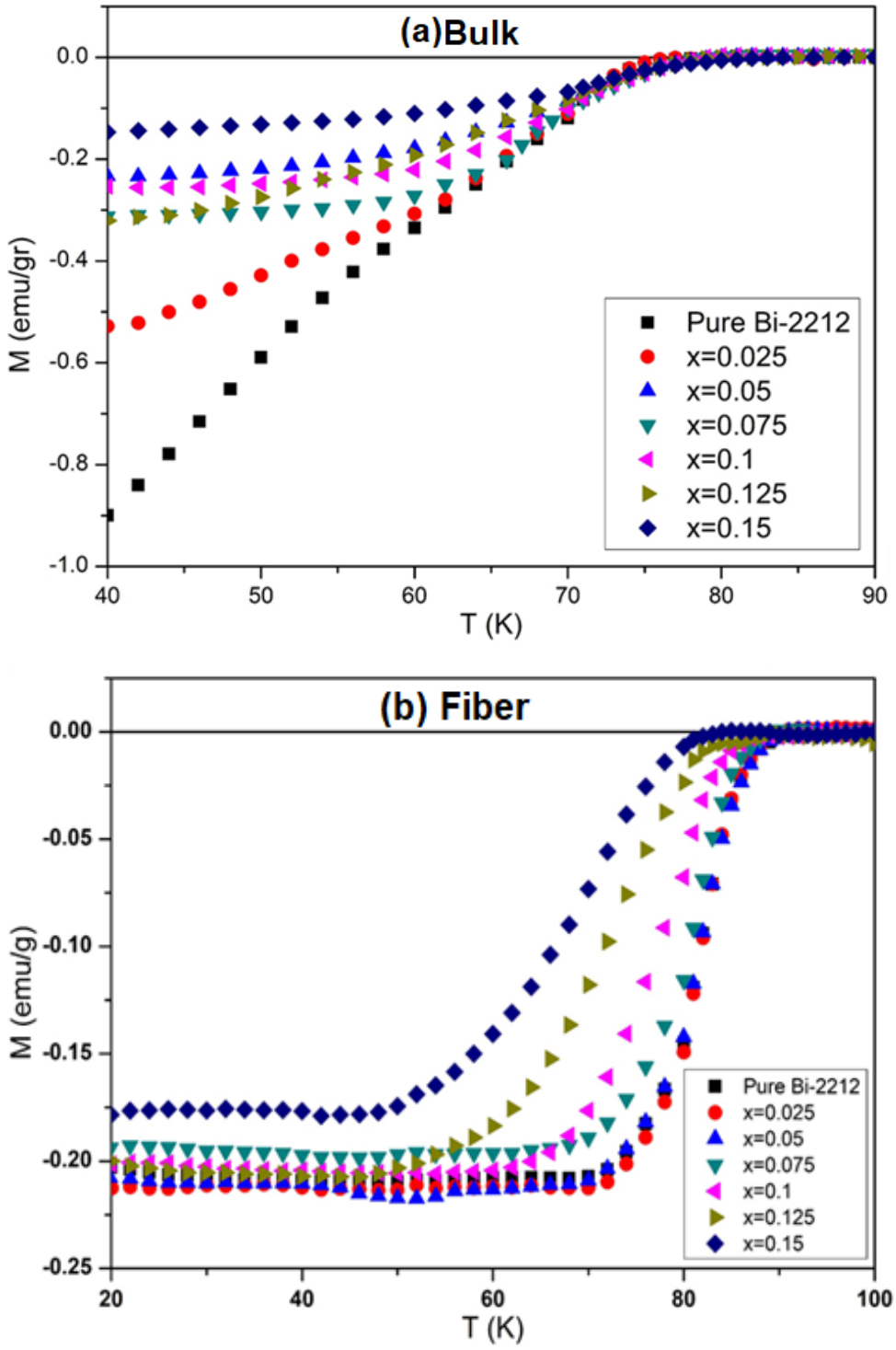
(a)Bulk
M (emu/gr)
T (K)
Pure Bi-2212
x=0.025
x=0.05
x=0.075
x=0.1
x=0.125
x=0.15
(b) Fiber
M (emu/g)
T (K)
Pure Bi-2212
x=0.025
x=0.05
x=0.075
x=0.1
x=0.125
x=0.15

Figure 4

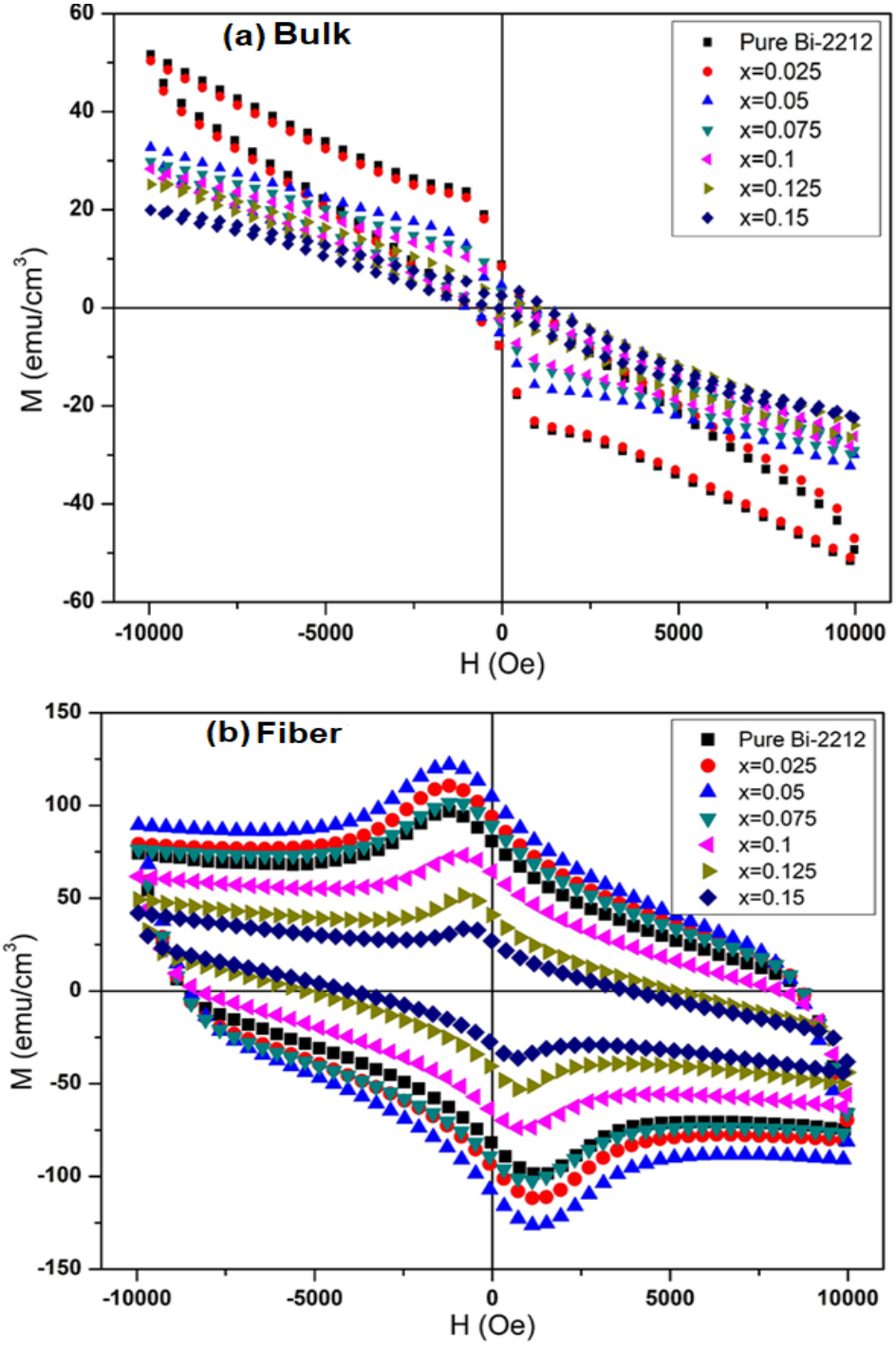
(a) Bulk
Pure Bi-2212
x=0.025
x=0.05
x=0.075
x=0.1
x=0.125
x=0.15
M (emu/cm^3)
H (Oe)
60
40
20
0
-20
-40
-60
-10000
-5000
0
5000
10000
(b) Fiber
Pure Bi-2212
x=0.025
x=0.05
x=0.075
x=0.1
x=0.125
x=0.15
M (emu/cm^3)
H (Oe)
150
100
50
0
-50
-100
-150
-10000
-5000
0
5000
10000

Figure 5

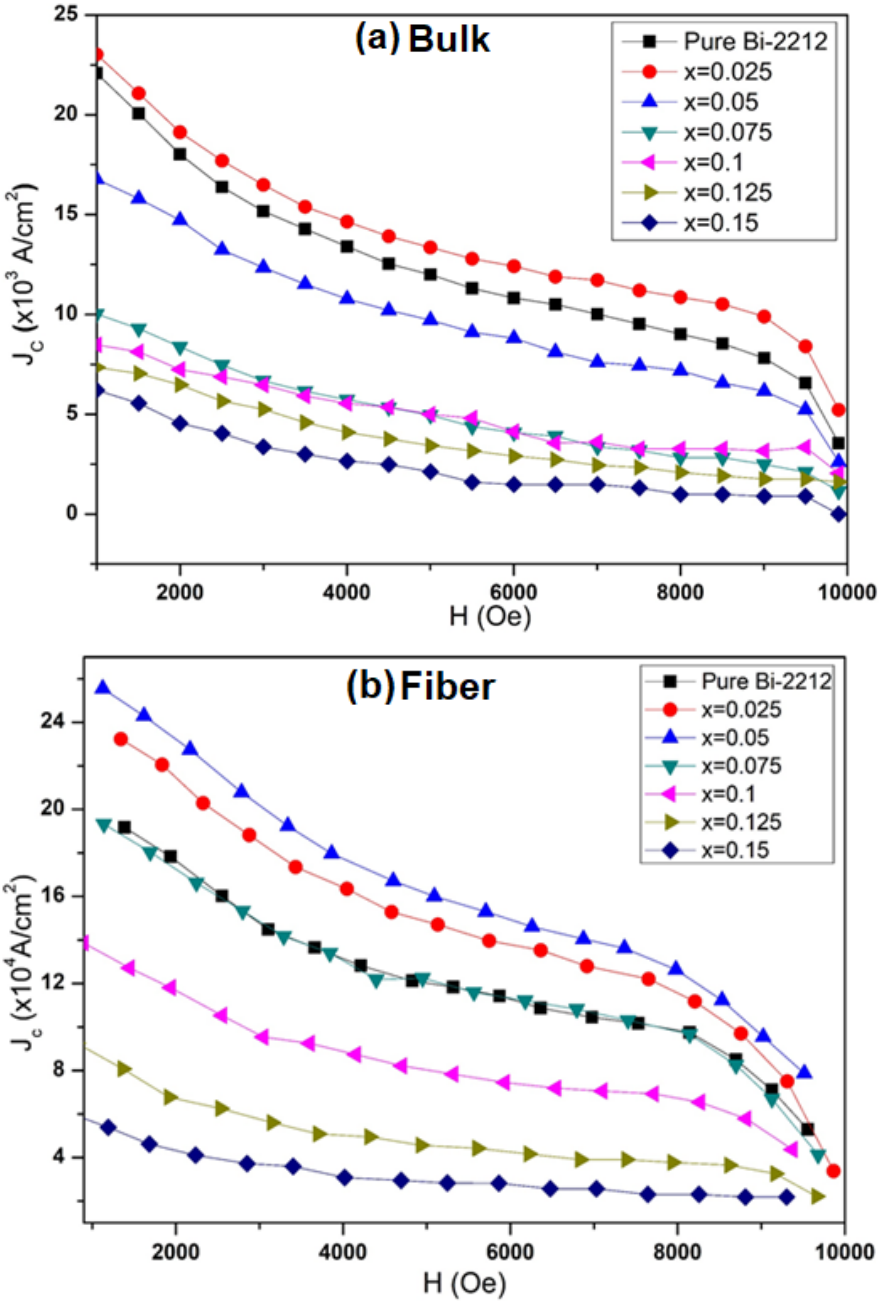
(a) Bulk
Pure Bi-2212
x=0.025
x=0.05
x=0.075
x=0.1
x=0.125
x=0.15
J_C (x10^3 A/cm^2)
H (Oe)
(b) Fiber
Pure Bi-2212
x=0.025
x=0.05
x=0.075
x=0.1
x=0.125
x=0.15
J_c (x10^{4}A/cm^2)
H (Oe)

Figure 6

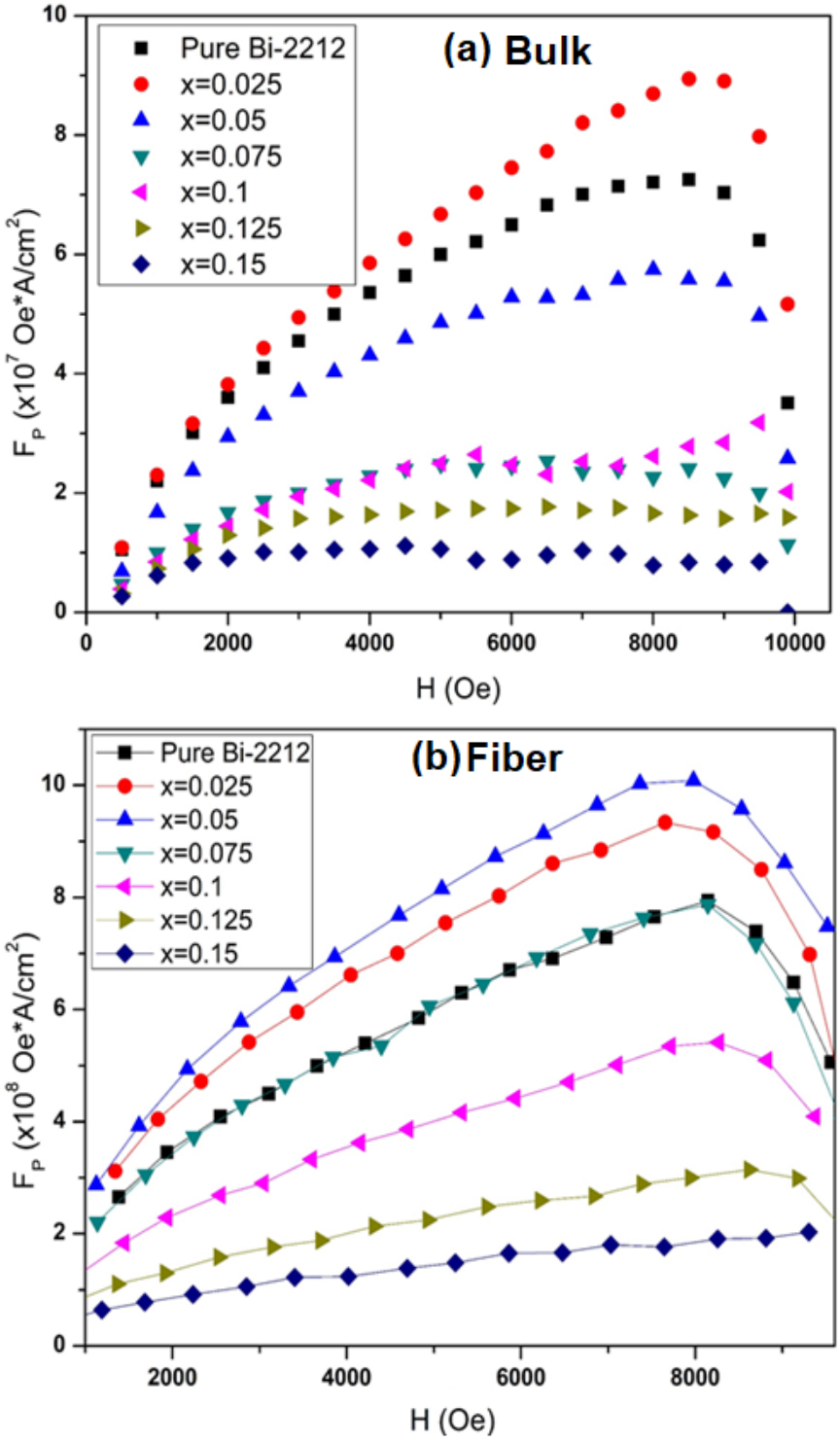
(a) Bulk
Pure Bi-2212
x=0.025
x=0.05
x=0.075
x=0.1
x=0.125
x=0.15
F_P (x10^7 Oe*A/cm^2)
H (Oe)
0
2000
4000
6000
8000
10000
(b) Fiber
Pure Bi-2212
x=0.025
x=0.05
x=0.075
x=0.1
x=0.125
x=0.15
F_P (x10^8 Oe*A/cm^2)
H (Oe)
2000
4000
6000
8000

Figure 7

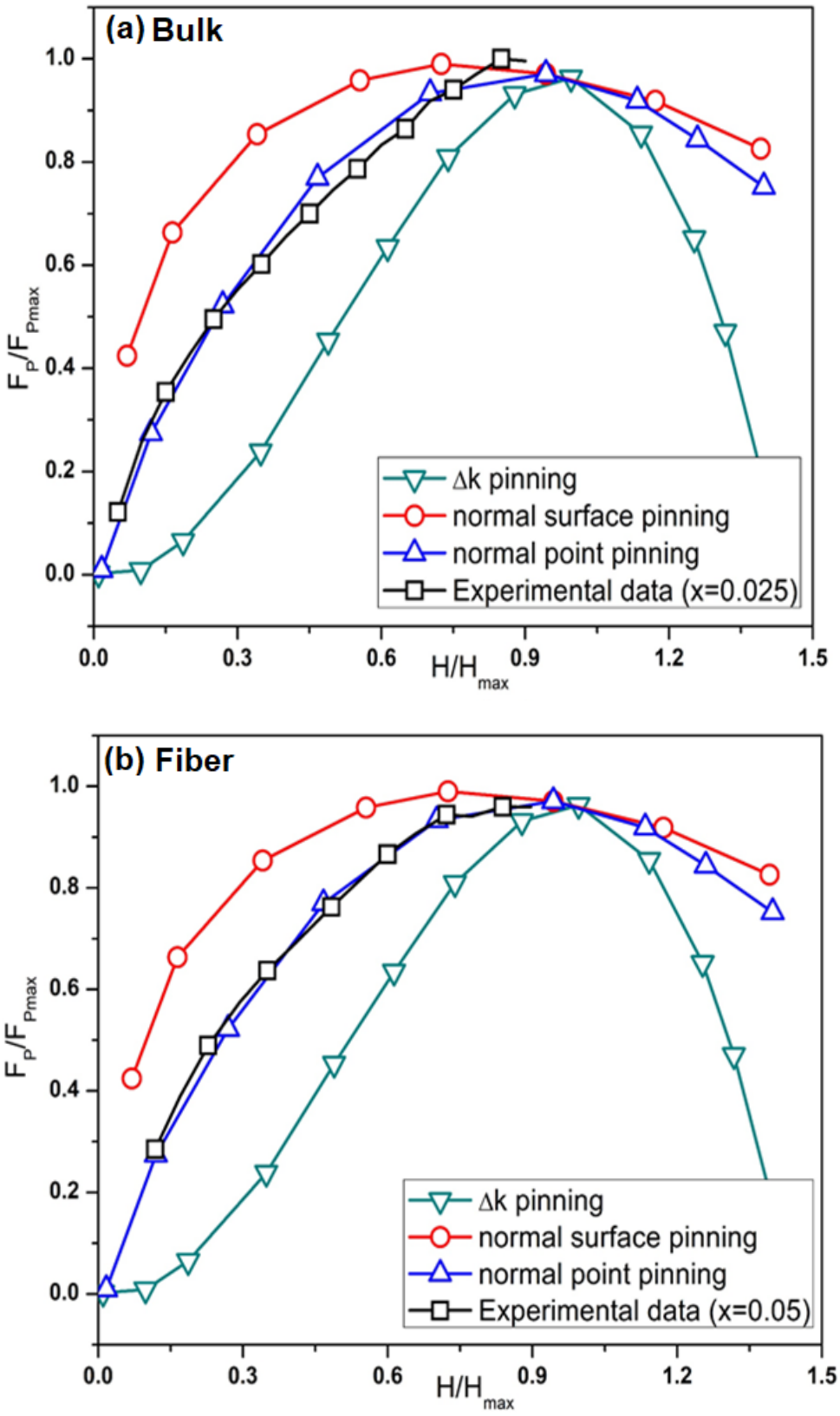
(a) Bulk
1.0
0.8
0.6
0.4
0.2
0.0
F_P/F_Pmax
0.0
0.3
0.6
0.9
1.2
1.5
H/H_max
Δk pinning
normal surface pinning
normal point pinning
Experimental data (x=0.025)
(b) Fiber
1.0
0.8
0.6
0.4
0.2
0.0
F_P/F_Pmax
0.0
0.3
0.6
0.9
1.2
1.5
H/H_max
Δk pinning
normal surface pinning
normal point pinning
Experimental data (x=0.05)